ACS APPLIED MATERIALS & INTERFACES

Research Article

www.acsami.org

Hierarchical CdS Nanowires Based Rigid and Flexible Photodetectors with Ultrahigh Sensitivity

Ludong Li,[†] Zheng Lou,[†] and Guozhen Shen*

State Key Laboratory for Superlattices and Microstructures, Institute of Semiconductors, Chinese Academy of Sciences, Beijing 100083, China

Supporting Information

ABSTRACT: Hierarchical CdS nanowires were synthesized via a facile vapor transport method, which were used to fabricate both rigid and flexible visible-light photodetectors. Studies found that the rigid photodetectors on SiO_2/Si substrate showed ultrahigh photo-dark current ratio up to 1.96×10^4, several orders of magnitude higher than previously reported CdS nanostructures, as well as high specific detectivity (4.27×10^{12} Jones), fast response speed and excellent environmental stability. Highly flexible photodetectors were also fabricated on polyimide substrate, which exhibited comparable photoresponse performance as the rigid one. In addition, the as-prepared flexible devices displayed excellent mechanical flexibility, electrical stability and folding endurance. The results indicate that the hierarchical CdS nanowires may be good candidates for nanoscale optoelectronic devices such as high-efficiency photoswitches and highly photosensitive detectors.

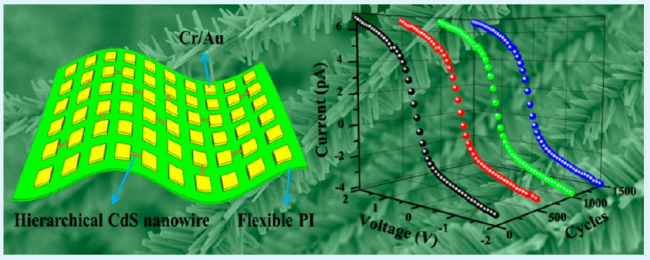

KEYWORDS: *hierarchical nanowires, CdS, photodetectors, flexible electronics, ultrahigh sensitivity*

1. INTRODUCTION

With large surface-to-volume ratio, high aspect ratio, and surface with dangling bonds that can be easily modified and functionalized, one-dimensional (1D) inorganic semiconductor nanostructures have been extensively studied as key units in transistors, photodetectors, lasers, chemical/biosensors, solar cells, lithium-ion batteries and supercapacitors.[1−10] Among them, photodetectors have been paid great attention because of their potential applications in optical communication, optical interconnects, optical switches, and high-resolution image sensing techniques.[10−13] Until now, many kinds of 1D inorganic semiconductor nanostructures have been used as the active materials for photodetectors and devices based on these nanostructures usually exhibit much better performance compared with those based on block or thin film materials due to their large specific surface area and small size that is comparable to the Debye length.[8,14−16]

With a direct bandgap of ~2.4 eV, relative low work function, high refraction index and excellent transport properties, CdS is a very promising material for visible-light photodetectors and several kinds of 1D CdS nanostructures have been used to fabricate visible-light photodetectors.[17−19] For example, Gupta et al. reported single CdS nanorod photodetectors passivated by oxygen, which displayed stable $I-V$ characteristics in dark and light conditions under a wide temperature range.[19] Wang et al. fabricated individual Schottky-gated CdS nanowire photodetectors, which showed much higher detection sensitivity and shorter reset time.[20] Li et al. constructed single CdS-nanobelt photodetectors, which exhibited an ultrafast response time and ultrahigh quantum efficiency.[21] Although these devices exhibited improved photoresponse performance, the detection sensitivity is still quite low, which greatly limits their practical application. Therefore, it is important and meaningful to find an effective wayto enhance the photo-dark current ratio of 1D CdS based detectors.

It is well-known that the morphology has an important effect on the properties of the active material, and compared with simple nanowires, hierarchical branched nanowires can provide much larger specific surface area for light absorption and more effective channels for photogenerated carrier transport, which may be useful to enhance the photo-dark current ratio of photodetectors.[22−26] It is thus postulated that if hierarchical CdS nanowires can be synthesized and applied to photodetectors, the photoresponse performance of devices will get a great improvement.

In this work, hierarchical branched CdS nanowires were synthesized via a facile vapor transport method, which can be used to fabricate photodetectors on both rigid SiO_2/Si substrate and flexible polyimide (PI) substrate. Both of them showed greatly improved photo-dark current ratios as well as fast response speed and excellent environmental stability. Besides, the flexible devices exhibited an outstanding mechanical flexibility, electrical stability and folding endurance.

Received: July 7, 2015
Accepted: October 6, 2015
Published: October 6, 2015

DOI: 10.1021/acsami.5b06070
ACS Appl. Mater. Interfaces 2015, 7, 23507−23514

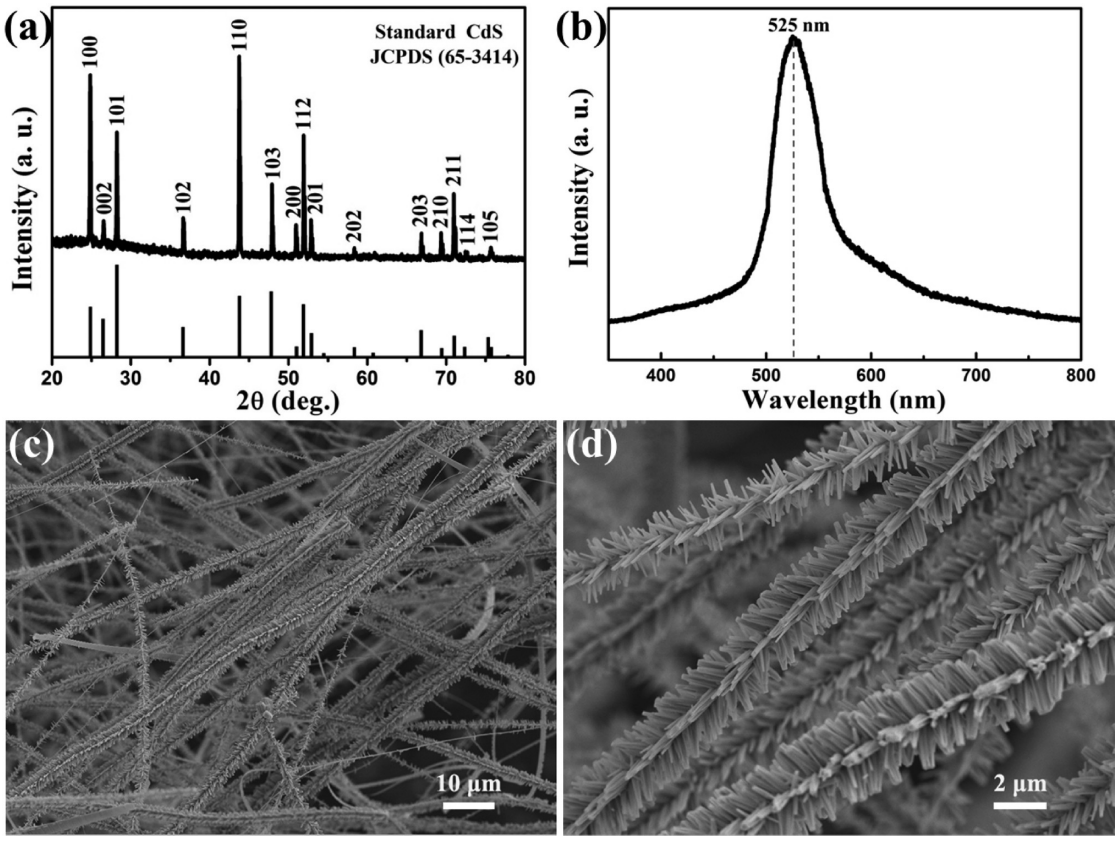

Figure 1. (a) XRD pattern, (b) PL spectra, (c,d) SEM images of the as-synthesized hierarchical CdS nanowires.

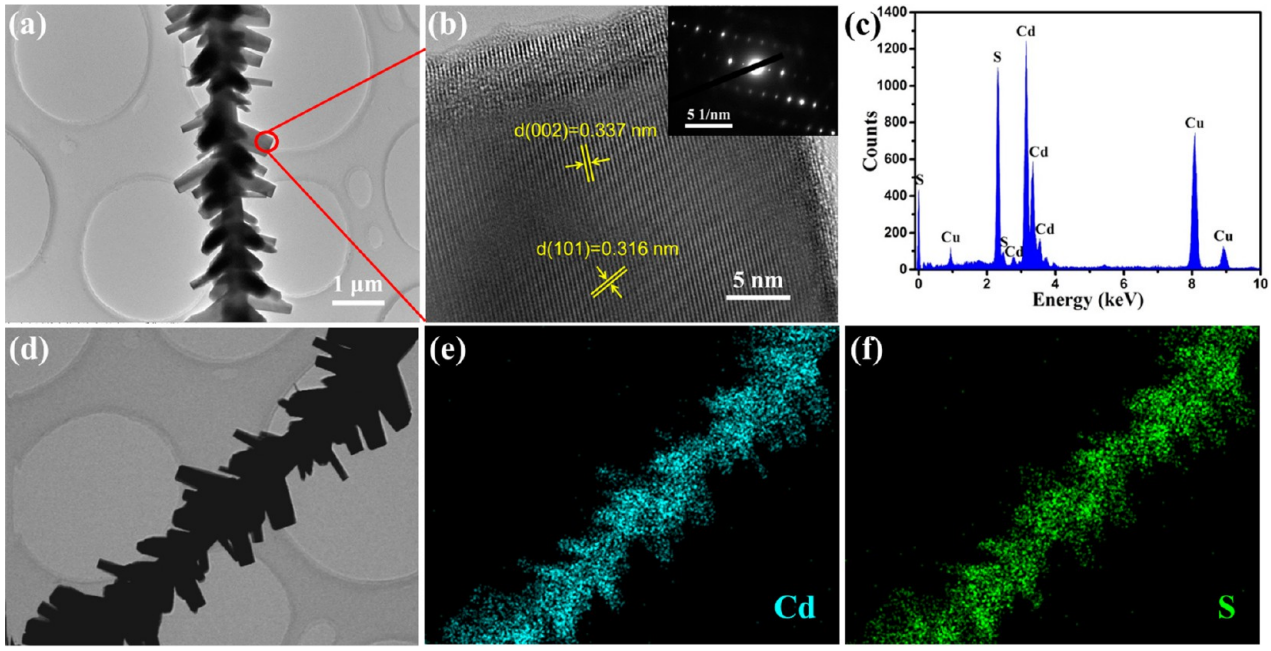

Figure 2. (a) TEM image, (b) HRTEM image of the as-synthesized hierarchical CdS nanowires. The inset is the corresponding SAED pattern. (c) EDX spectrum recorded from the hierarchical CdS nanowires. (d–f) STEM image and corresponding elemental mapping showing the dispersion of Cd and S element in hierarchical CdS nanowires.

2. EXPERIMENTAL SECTION

Preparation and Characterization of Hierarchical CdS Nanowires. The hierarchical CdS nanowires in this work were synthesized via a simple vapor transport method, which is similar to the previous reports.[26] In a typical process, 0.075 g of CdS powder (99.999%) was placed on an alumina boat at the center of a tube furnace as the source material. A silicon wafer coated with ~10 nm thick Au layer as the catalysts was placed on the other alumina boat located downstream, at a distance of 16–17 cm from the tube center. After the tube was purged with pure Ar at 110 °C for 2 h, the system was heated to 1000 °C in 35 min and maintained at that temperature

DOI: 10.1021/acsami.5b06070
ACS Appl. Mater. Interfaces 2015, 7, 23507–23514

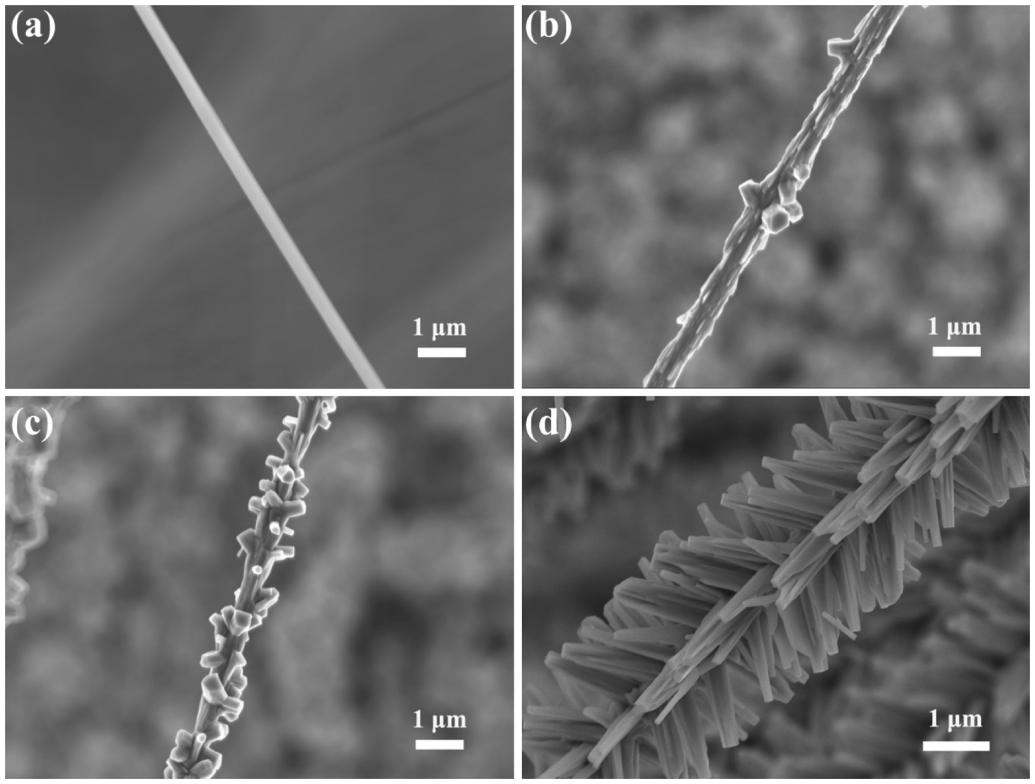

Figure 3. SEM images of the as-synthesized CdS nanowires under the different growth times: (a) 10 min, (b) 0.5 h, (c) 1 h and (d) 2 h.

for 2 h. The flow rate of the carrier gas (Ar) was kept at 300 sccm (standard cubic centimeters per minute). After the reaction ended, the furnace was cooled down to room temperature naturally. The products were characterized by powder X-ray diffractometer (XRD, Rigaku D/Max-2550, λ = 1.5418 Å), scanning electron microscopy (SEM, Zeiss Supra55(VP)), transmission electron microscopy (TEM, JEM-2100F) with an energy-dispersive X-ray (EDX) analyzer and room temperature photoluminescence (PL) (Horiba JY HR800) with an excitation laser (Kimmon He−Cd laser) of 325 nm.

Device Fabrication and Measurements. To fabricate photodetectors, the hierarchical CdS nanowires were first transferred to either a rigid SiO_2/Si substrate or a flexible PI substrate by the contact printing method. Then using the conventional photolithography, thermal evaporation, and lift-off process, the Cr/Au (10/100 nm) electrodes were patterned on top of the hierarchical nanowires. The photoresponse properties of the devices were measured by the Keithley 4200-SCS semiconductor characterization system that linked with a probe station. A power adjustable homogeneous light source system was used as the illumination source for photoresponse measurements. The incident power of the light was measured using an Ophir NOVA power meter. The vacuum $I-V$ tests of the devices were measured by the Agilent B1500A semiconductor device analyzer that linked with a cryogenic vacuum probe station (Lake Shore CRX-4K). The above measurements were performed at room temperature.

3. RESULTS AND DISCUSSION

Figure1a is the XRD pattern of the as-synthesized products. All of the observed peaks can be indexed to the hexagonal wurtzite CdS (JCPDS Card No. 65-3414). Figure 1b depicts the room temperature PL spectra of single crystalline hierarchical CdS nanowires. A strong emission peak located at wavelength 525 nm was observed in the test range from 350 to 800 nm. So, the bandgap of the as-synthesized hierarchical CdS nanowires can be calculated as ∼2.4 eV, corresponding to previous reports.[18,21] Figure 1c,d displays the SEM images with different magnifications, where hierarchical nanowires can be seen on a large scale after reaction. The backbones of the hierarchical CdS nanowires have a length of more than 100 μm and a diameter of 300−400 nm, whereas the lengths of the CdS nanorod branches grown on the CdS backbones range from 1 to 2 μm and their diameters are about 200−300 nm.

Figure 2a,b depicts the TEM image and the high-resolution TEM (HRTEM) image of an individual hierarchical CdS nanowire, respectively. The HRTEM image was taken from the red-circle area shown in Figure 2a, which shows its single-crystalline nature, corresponding to the SAED pattern inset in Figure 2b. The lattice spacing observed from the HRTEM image was 0.337 and 0.316 nm, in agreement with the (002) and (101) planes of hexagonal wurtzite CdS phase. The energy dispersive X-ray (EDX) spectrum shown in Figure 2c reveals that the hierarchical nanowire is consisted of Cd and S elements, considering that the signal from Cu element is from the TEM grid. This can be further confirmed by the scanning TEM (STEM) and the corresponding EDX elemental mapping shown in Figure 2d−f.

Hierarchical CdS nanowires were fabricated via a simple vapor transport method using Au layer as seed layers. This is a very standard vapor−liquid−solid (VLS) technique for the growth of one-dimensional nanostructures, like nanowires and nanorods. However, in the present case this technique results in hierarchical structure. To study the growth mechanism of hierarchical CdS nanowires, CdS nanowires were synthesized by the same method with just different growth time (10 min, 0.5 h, 1 and 2 h), as shown in Figure 3. From Figure 3a−d, the growth mechanism of hierarchical CdS nanowires can be explained as follows. First, CdS nanowires were synthesized as the backbones via the standard VLS mechanism (Figure 3a). Then, as the transport and deposition of CdS vapor, the surface of CdS nanowires became rough (Figure 3b), which is good for nucleating of CdS in the surface of CdS nanowires. Finally, as

DOI: 10.1021/acsami.5b06070
ACS Appl. Mater. Interfaces 2015, 7, 23507−23514

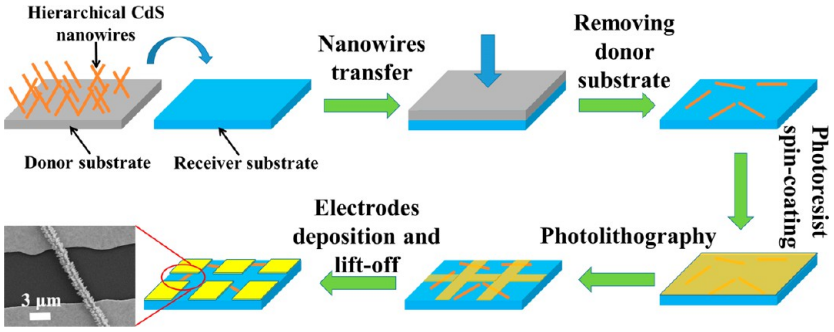

Figure 4. Schematic illustration of the fabrication process of hierarchical CdS nanowire photodetectors. The inset is the SEM image of the photodetector.

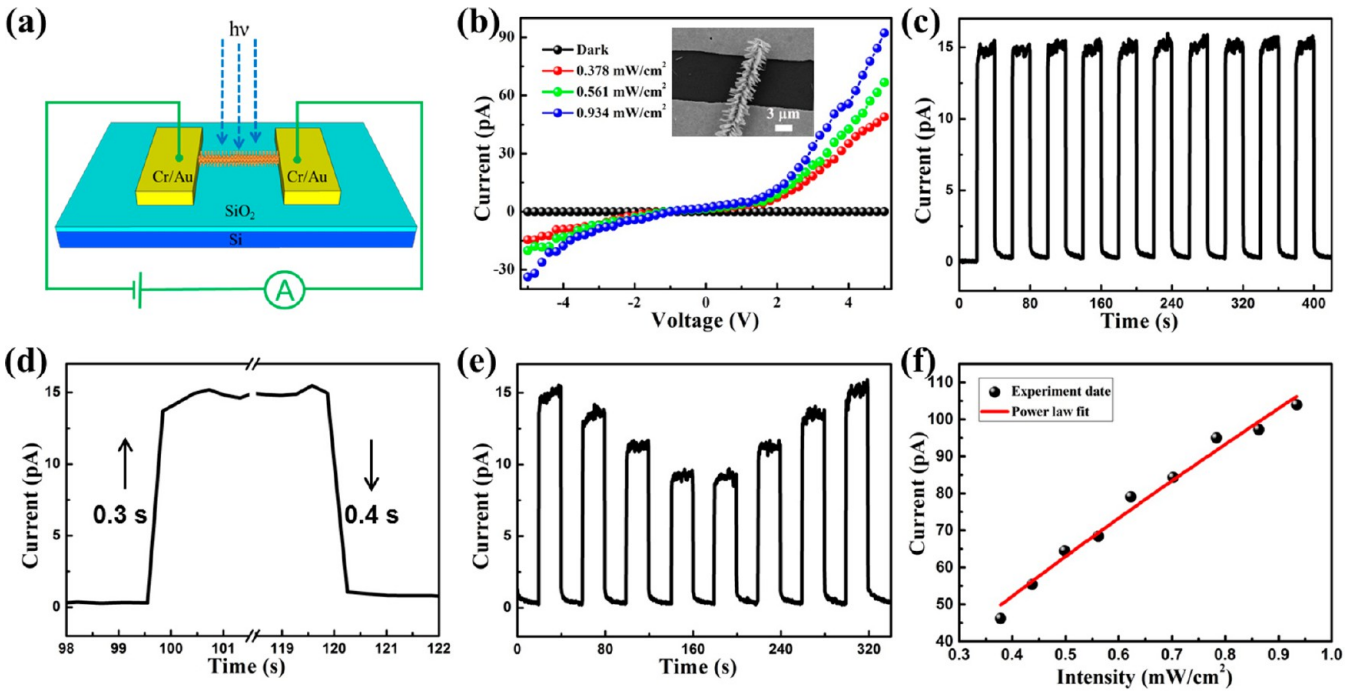

Figure 5. (a) Schematic illustration of as-fabricated photodetector on SiO_2/Si substrate. (b) I−V test result of the device under different power intensities of 470 nm light illumination and in dark. The inset is the SEM image of the photodetector. (c) Photoresponse characteristics of the device at a bias of 2 V with a light intensity of 0.934 mW/cm^2. (d) Enlarged view of one cycle in (c). (e) Photoresponse characteristics of the device at a bias of 2 V with different light intensities. (f) The dependence of photocurrent on light intensity. The fitting result is $I \sim P^{0.84}$.

the growth time increased, CdS crystal nucleuses grew continuously in the surface of CdS nanowires to form side branches (Figure 3c,d).[27,28] It can be seen that enough growth time and material supply are important for the synthesis of hierarchical CdS nanowires.

To study the photoresponse characteristics of the hierarchical CdS nanowires, individual hierarchical nanowire photodetectors on rigid SiO_2/Si substrate were fabricated by a conventional photolithographic process. The fabrication process of hierarchical CdS nanowire photodetectors is shown in Figure 4. To fabricate hierarchical CdS nanowire photodetectors, the donor substrate (Si substrate) that grew hierarchical CdS nanowires was first attached to the receiver substrate (SiO_2/Si substrate) under a certain pressure. By peeling the donor substrate off the receiver substrate, the hierarchical CdS nanowires were successfully transferred to the surface of the receiver substrate. Then using the conventional photolithography, thermal evaporation, and lift-off process, the Cr/Au (10/100 nm) electrodes were patterned on top of the hierarchical nanowires. The gap between two electrodes was about 10 μm. The SEM image of as-fabricated individual hierarchical CdS nanowire photodetector is shown in the inset of Figure 4.

Figure 5a shows the schematic illustration of the as-fabricated device. We used the monochromatic light as the irradiated light, and the corresponding photoresponse signals were recorded. Figure 5b illustrates the $I-V$ plots of the photodetector in the dark and under different power intensities of 470 nm light illumination (from 0.378 to 0.934 mW/cm^2). We can observe that the photocurrent significantly increases with the light intensity increases at the identical voltage, which is because the charge carrier photogeneration efficiency increases as the increasing of the absorbed photon flux. When the device was under a visible light of 470 nm with a light intensity of 0.934 mW/cm^2 at a bias voltage of 5 V, the light current was about 92.2 pA. However, at the same bias voltage of 5 V, the dark current of the device was only 4.7 fA. The photo-dark current ratio (I_{light}/I_{dark}) of the device was up to 1.96×10^4, which is several orders of magnitude higher than the previously reported

DOI: 10.1021/acsami.5b06070
ACS Appl. Mater. Interfaces 2015, 7, 23507−23514

Table 1. Comparison of the Critical Parameters for the Present Hierarchical CdS Nanowire and Previous CdS-Nanostructure Photodetectors

CdS PDs	wavelength and intensity of light	I_{light}/I_{dark}	response time	reference
nanorod	400 nm	<40	2.3 s	19
nanowire	365 nm	<200	0.380 s	20
nanobelt	490 nm; 3.0 mW/cm^2	6	20 μs	21
nanowire	405 nm; 16 mW/cm^2	30	0.267 s	29
nanowire	500 nm; 3.25 mW/cm^2	230	1.4 ms	30
nanobelt	white light (10 W)	<3000	1 s	31
hierarchical NWs	470 nm; 0.934 mW/cm^2	1.96×10^4	0.3 s	this work

CdS-nanostructure photodetectors, as summarized in Table 1.[19−21,29−31] At the same time, Table 1 also exhibits that the intensity of monochromatic light (0.934 mW/cm^2) that we used in $I-V$ curve test is very weak. That means the single hierarchical CdS nanowire photodetector can reach a very high photo-dark current ratio even in a weak light intensity, which further proves the ultrahigh sensitivity of the hierarchical CdS nanowire photodetector. As a contrast, individual CdS nanowire (without branches) photodetectors on rigid SiO_2/Si substrate were fabricated by the same photolithographic process. The $I-V$ plots of the photodetector in the dark and under 470 nm light illumination with a light intensity of 0.934 mW/cm^2 is shown in Figure S1. At a bias voltage of 5 V, the light current of the device was about 11.9 pA and the dark current was about 107.7 fA, so the photo-dark current ratio of the device was only 110. It can be seen that, compared with the CdS nanowire photodetector, the hierarchical nanowire photodetector possessed much smaller dark current and much larger light current, which can be explained as follows.

On one hand, the surface of the nanowire exposed to the air will adsorb many oxygen molecules. Because of the large specific surface area, the conductivity of the nanowire can be affected intensively by the adsorption and desorption of oxygen. To see the effect of oxygen to the conductivity of the device, a control experiment that testing the $I-V$ curves of the device in air and vacuum (0.1 Pa) without light illumination was done and given in the Supporting Information. As shown in Figure S2, the dark current of the device in a vacuum is much higher than the dark current in air after 7 V, which proves the adsorption of oxygen molecules can increase the resistance of the nanowire. The obvious fluctuation of the dark current in vacuum is because the vacuum $I-V$ test of the device was measured by the Agilent B1500A semiconductor device analyzer, which has a lower current resolution than the Keithley 4200-SCS. As a further explanation, because of the larger electronegativity, oxygen molecules adsorbed on the surface of the nanowire can capture free electrons and form a depletion layer at the surface of the nanowire and then increase the resistance of the nanowire.[32] The hierarchical CdS nanowire has much larger specific surface area, which can adsorb more oxygen molecules and lead to a higher resistance and smaller dark current compared to conventional CdS nanowire. On the other hand, when the device was illuminated by visible-light, electron−hole pairs were therefore generated and then negative oxygen ions trapped holes and desorbed from the surface of the nanowire, which can reduce the thickness of the depletion layer obviously and increase the conductivity of the nanowire enormously.[32] Consequently, the hierarchical CdS nanowire photodetector possessed much larger photocurrent because the hierarchical nanowire can provide much larger specific surface area for light absorption and more effective channels for photogenerated carriers transport.[22−26] In addition, the multiple light scattering among the CdS nanorod branches can further heighten the light absorption of hierarchical CdS nanowires.

As another key parameter, specific detectivity (D^*) can also reflect the detection sensitivity of a photodetector to incident light and it can be expressed by the equations:[33,34]

$$D^* = \frac{(\Delta f A)^{1/2}}{\mathrm{NEP}} \ (\mathrm{cm\ Hz^{1/2}\ W^{-1}} = \mathrm{Jones}) \tag{1}$$

$$\mathrm{NEP} = \frac{i_n}{R_\lambda} = \frac{i_n}{(\Delta I/PA)} \ (\mathrm{W}) \tag{2}$$

where NEP is the noise equivalent power, A is the effective area of the detector, Δf is the bandwidth, R_λ is the responsivity, i_n is the noise current, ΔI is the photocurrent and P is the incident light intensity. If the shot noise from the dark current is the major contribution to the noise limit of the detectivity, the specific detectivity can be simplified as[33,34]

$$D^* = \frac{(\Delta I/PA)}{(2eI_{dark}/A)^{1/2}} \tag{3}$$

Calculated from the above equations, at a bias voltage of 5 V, the specific detectivity of our hierarchical CdS nanowire photodetector was up to 4.27×10^{12} Jones under 470 nm light with a light intensity of 0.934 mW/cm^2, which confirms the ultrahigh sensitivity of the hierarchical CdS nanowire photodetector again.

The dynamic photocurrent response of the single hierarchical CdS nanowire photodetector is displayed in Figure 5c, which is measured by periodically turning on and off a 470 nm light with a light intensity of 0.934 mW/cm^2 at a bias voltage of 2 V. From the curve, we can see that the photocurrent increases quickly and reaches steady state when the light is turned on and then decreases rapidly after the light is turned off, revealing the superior response and stability of the device. Figure 5d shows an enlarged view of one cycle in Figure 5c, and the rise and decay times were about 0.3 and 0.4 s, respectively, here the rise and decay time defined as the peak value from 10% to 90% (90% to 10%) of the photocurrent. We also measured two cycles of the $I-T$ curve under different power intensities of 470 nm light illumination at a bias voltage of 2 V, as shown in Figure 5e. It can be seen that the saturated photocurrent decreases as the diminution of light intensity, and then recovers much the same value as the recovery of light intensity, indicating the good reproducibility of the photodetector. Figure 5f describes the relationship of photocurrent versus light intensity at a bias voltage of 5 V, which can be expressed with a power law, $I = AP^\theta$,[35] where I is the light current, A is a constant, P is the light intensity and θ is an empirical value. The

DOI: 10.1021/acsami.5b06070
ACS Appl. Mater. Interfaces 2015, 7, 23507−23514

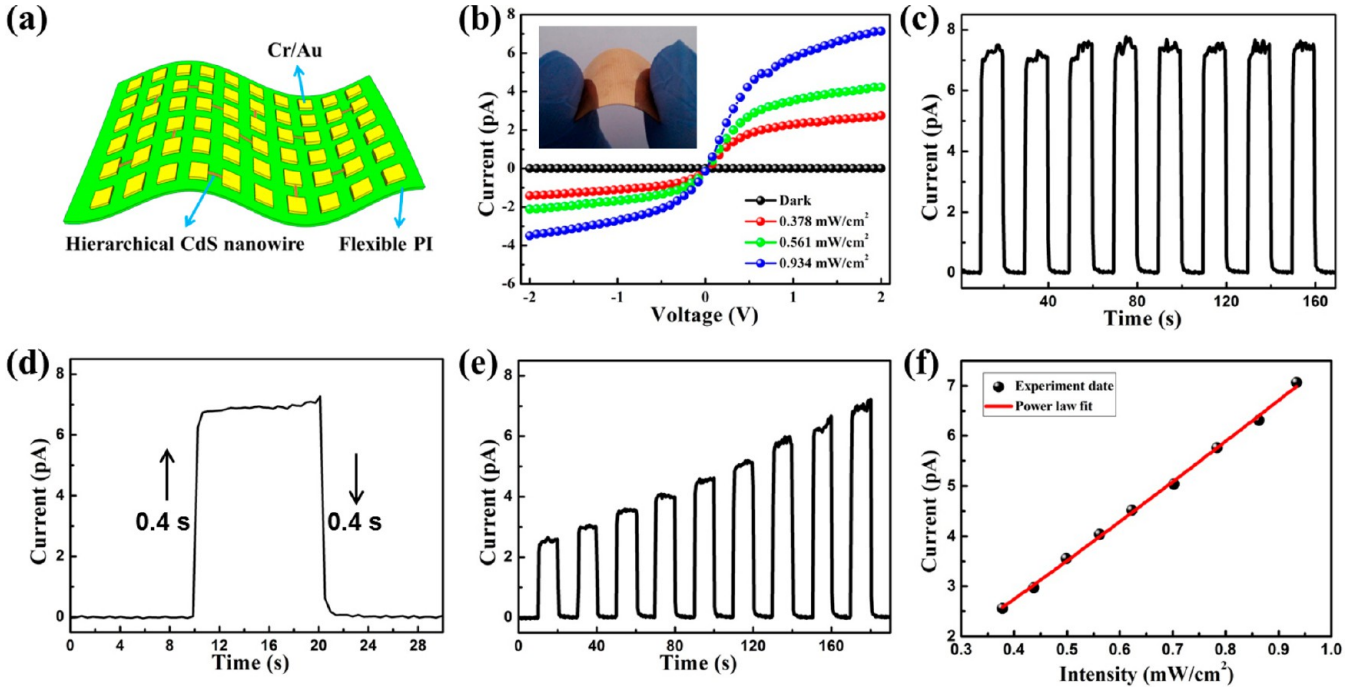

Figure 6. (a) Schematic illustration of as-fabricated flexible photodetectors on PI substrate. (b) $I-V$ test result of the device under different power intensities of 470 nm light illumination and in the dark. The inset is the optical image of the photodetectors. (c) Photoresponse characteristics of the device at a bias of 2 V with a light intensity of 0.934 mW/cm^2. (d) Enlarged view of one cycle in panel c. (e) Photoresponse characteristics of the device at a bias of 2 V with different light intensities. (f) Corresponding dependence of photocurrent on light intensity. The fitting result is $I \sim P^{1.10}$.

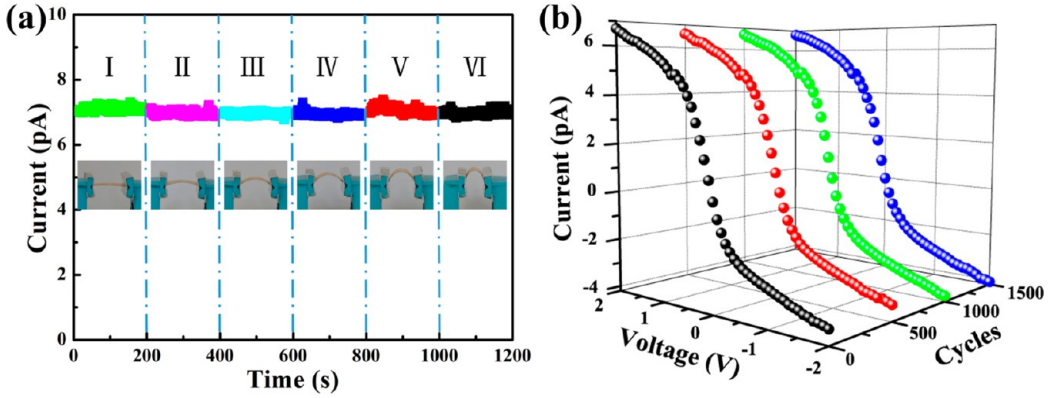

Figure 7. (a) $I-T$ curves of the flexible photodetector bent with different bending conditions under a bias voltage of 2 V. The lower section describes the currents measured at six different bending states. (b) $I-V$ curves of the flexible device under 470 nm light illumination after 0, 500, 1000 and 1500 cycles of bending.

fitting of the experimental values gave an exponential function of $I \sim P^{0.84}$, suggesting the excellent photocurrent capability of the hierarchical CdS nanowires.

Because of the portable, lightweight and foldable characteristics, flexible electronics have obtained great research interest and considerable development in the recent years.[1,10,15] Flexible photodetectors have also been studied made with many different organic or inorganic thin-film materials.[36,37] To study the potential applications of hierarchical CdS nanowires in flexible photodetectors, we used individual hierarchical CdS nanowire as the active material and PI as a flexible substrate to fabricate individual nanowire flexible photodetectors. Figure 6a is the schematic illustration of the device, in which every photodetector consists of a single hierarchical CdS nanowire and two electrodes (Cr/Au, 10/100 nm) connected with each end of the nanowire. The inset in Figure 6b is the optical image of the device, which shows the good flexibility of the device. Figure 6b shows the $I-V$ curves of the flexible photodetector under different power intensities of 470 nm light illumination and in dark. It can be observed that the current increases dramatically when the device was exposed to 470 nm light, which reveals that the flexible photodetector also has an excellent sensitivity. The $I-T$ curve of the flexible photodetector at a bias voltage of 2 V with a light intensity of 0.934 mW/cm^2 is displayed in Figure 6c. From the curve, we can see that the stability and reproducibility of the flexible photodetector are also good. The photo-dark current ratio of the flexible photodetector is more than 2500 and the response and recovery times are both 0.4 s (Figure 6d) at the applied voltage of 2 V. The trend of these results on the flexible PI substrate agrees well with those on the rigid SiO_2/Si substrate. Figure 6e exhibits the $I-T$ curve of the flexible photodetector under

DOI: 10.1021/acsami.5b06070
ACS Appl. Mater. Interfaces 2015, 7, 23507−23514

different light intensities of 470 nm light illumination. At a bias voltage of 2 V, the saturated photocurrent increases gradually with the uniform increase of light intensity, which implies the relationship between photocurrent and light intensity is approximately linear. The corresponding dependence of photocurrent on light intensity is fitted in Figure 6f. The fitting result is $I \sim P^{1.10}$, indicating the outstanding photocurrent capability of the hierarchical CdS nanowires again.

As a key parameter of the flexible electric devices' quality, the electrical stability is important for the future application of the flexible electric devices. The electrical stability of our flexible photodetectors was also investigated here. Figure 7a shows the $I-T$ curves of the flexible photodetector bent with different bending conditions under a bias voltage of 2 V. As shown in those insets in the lower section of Figure 7a, the bending curvature of the flexible device can be controlled by changing the distance of two mechanical stages. It can be observed that the photocurrent nearly maintained the same value at six different bending states (the insets in Figure7a), which demonstrates the fact that the bending stress had almost no effect on the conductance of the flexible photodetector. This result reveals that our flexible photodetector has a superior mechanical flexibility and electrical stability. Besides the electrical stability, the folding endurance is also a key factor affecting the practical application of the flexible electric devices. We defined that the flexible device have been bent from states I to VI (Figure 7a) and then recovered to state I was one cycle. Figure 7b exhibits the $I-V$ curves of the flexible photodetector after different cycles of bending, which was tested under 470 nm light illumination with a light intensity of 0.934 mW/cm^2. It can be seen that even after 500, 1000 and 1500 cycles of bending, the $I-V$ curves of the flexible photodetector were still almost unchanged compared to the $I-V$ curve without bending, indicating the excellent folding endurance of the hierarchical CdS nanowire flexible photodetector.

4. CONCLUSION

In summary, single-crystalline hierarchical CdS nanowires were synthesized via a facile vapor transport method, and the possible growth mechanism was discussed. The as-synthesized hierarchical CdS nanowires were used to fabricate both rigid and flexible visible-light photodetectors. Studies found that the rigid photodetectors on SiO_2/Si substrate showed ultrahigh photo-dark current ratio up to 1.96×10^4, several orders of magnitude higher than previously reported CdS nanostructures, as well as high specific detectivity (4.27×10^{12} Jones), fast response speed and excellent environmental stability. Highly flexible photodetectors were also fabricated on PI substrate, which exhibited comparable photoresponse performance as the rigid one. In addition, the as-prepared flexible devices displayed excellent mechanical flexibility, electrical stability and folding endurance. The results indicate that the hierarchical CdS nanowires may be good candidates for nanoscale optoelectronic devices such as high-efficiency photoswitches and highly photosensitive detectors.

■ ASSOCIATED CONTENT

Supporting Information

The Supporting Information is available free of charge on the ACS Publications website at DOI: 10.1021/acsami.5b06070.

$I-V$ plots of the photodetector based on CdS nanowire (without branches) in the dark and under 470 nm light illumination with a light intensity of 0.934 mW/cm^2; $I-V$ plots of the device in air and vacuum (0.1 Pa) without light illumination (PDF).

■ AUTHOR INFORMATION

Corresponding Author

*G. Shen. E-mail: gzshen@semi.ac.cn.

Author Contributions

†L. Li and Z. Lou contributed equally to this work. The paper was written through contributions of all authors. All authors have given approval to the final version of the paper.

Notes

The authors declare no competing financial interest.

■ ACKNOWLEDGMENTS

This work was supported by the National Natural Science Foundation (61377033).

■ REFERENCES

(1) Liu, Z.; Xu, J.; Chen, D.; Shen, G. Z. Flexible Electronics Based on Inorganic Nanowires. *Chem. Soc. Rev.* **2015**, *44*, 161−192.

(2) Lou, Z.; Li, L. D.; Shen, G. Z. $InGaO_3(ZnO)$ Superlattice Nanowires for High Performance Ultraviolet Photodetectors. *Adv. Electron. Mater.* **2015**, *1*, 1500054.

(3) Wang, L. L.; Deng, J. N.; Lou, Z.; Zhang, T. Cross-linked P-type Co_3O_4O ctahedron Nanoparticles in 1 D N-type TiO_2 Nanofibers for High-performance Sensing Devices. *J. Mater. Chem. A* **2014**, *2*, 10022−10028.

(4) Wang, Z. R.; Wang, H.; Liu, B.; Qiu, W. Z.; Zhang, J.; Ran, S. H.; Huang, H. T.; Xu, J.; Han, H. W.; Chen, D.; Shen, G. Z. Transferable and Flexible Nanorod-Assembled TiO_2 Cloths for Dye-Sensitized Solar Cells. *ACS Nano* **2011**, *5*, 8412−8419.

(5) Liu, B.; Zhang, J.; Wang, X. F.; Chen, G.; Chen, D.; Zhou, C. W.; Shen, G. Z. Hierarchical Three-Dimensional $ZnCo_2O_4$ Nanowire Arrays/Carbon Cloth Anodes for a Novel Class of High-Performance Flexible Lithium-ion Batteries. *Nano Lett.* **2012**, *12*, 3005−3011.

(6) Chen, Z.; Augustyn, V.; Wen, J.; Zhang, Y. W.; Shen, M. Q.; Dunn, B.; Lu, Y. F. High-Performance Supercapacitors Based on Intertwined CNT/V_2O_5 Nanowire Nanocomposites. *Adv. Mater.* **2011**, *23*, 791−795.

(7) Liu, X. Q.; Liu, X.; Wang, J. L.; Liao, C. L.; Xiao, X. H.; Guo, S. S.; Jiang, C. Z.; Fan, Z. Y.; Wang, T.; Chen, X. S.; Lu, W.; Hu, W. D.; Liao, L. High-Performance InGaZnO/Aligned-SnO_2 Nanowires Composite Thin-Film Transistors and Their Application in Photodetectors. *Adv. Mater.* **2014**, *26*, 7399−7404.

(8) Zhai, T. Y.; Li, L.; Wang, X.; Fang, X. S.; Bando, Y.; Golberg, D. Recent Developments in One-Dimensional Inorganic Nanostructures for Photodetectors. *Adv. Funct. Mater.* **2010**, *20*, 4233−4248.

(9) Miao, J. S.; Hu, W. D.; Guo, N.; Lu, Z. Y.; Zou, X. M.; Liao, L.; Shi, S. X.; Chen, P. P.; Fan, Z. Y.; Ho, J. C.; Li, T. X.; Chen, X. S.; Lu, W. Single InAs Nanowire Room-Temperature Near-Infrared Photodetectors. *ACS Nano* **2014**, *8*, 3628−3635.

(10) Chen, G.; Liang, B.; Liu, X.; Liu, Z.; Gang, Y.; Xie, X. M.; Luo, T.; Chen, D.; Zhu, M. Q.; Shen, G. Z.; Fan, Z. Y. High-Performance Hybrid Phenyl-C61-Butyric Acid Methyl Ester/Cd_3P_2Nanowire Ultraviolet−Visible−Near Infrared Photodetectors. *ACS Nano* **2014**, *8*, 787−796.

(11) Jie, J. S.; Zhang, W. J.; Jiang, Y.; Meng, X. M.; Li, Y. Q.; Lee, S. T. Photoconductive Characteristics of Single-Crystal CdS Nanoribbons. *Nano Lett.* **2006**, *6*, 1887−1892.

(12) Kind, H.; Yan, H. Q.; Messer, B.; Law, M.; Yang, P. NW Ultraviolet Photodetectors and Optical Switches. *Adv. Mater.* **2002**, *14*, 158−160.

(13) Fan, Z. Y.; Ho, J. C.; Jacobson, Z. A.; Razavi, H.; Javey, A. Large-Scale, Heterogeneous Integration of Nanowire Arrays for Image

DOI: 10.1021/acsami.5b06070
ACS Appl. Mater. Interfaces 2015, 7, 23507−23514

Sensor Circuitry. *Proc. Natl. Acad. Sci. U. S. A.* **2008**, *105*, 11066−11070.
(14) Fang, X. S.; Bando, Y.; Gautam, U. K.; Zhai, T. Y.; Zeng, H. B.; Xu, X. J.; Liao, M. Y.; Golberg, D. ZnO and ZnS Nanostructures: Ultraviolet-Light Emitters, Lasers, and Sensors. *Crit. Rev. Solid State Mater. Sci.* **2009**, *34*, 190−223.
(15) Wang, X.; Liu, B.; Liu, R.; Wang, Q.; Hou, X.; Chen, D.; Wang, R.; Shen, G. Z. Fiber-Based Flexible All-Solid-State Asymmetric Supercapacitors for Integrated Photodetecting System. *Angew. Chem., Int. Ed.* **2014**, *53*, 1849−1884.
(16) Zhai, T. Y.; Li, L.; Ma, Y.; Liao, M. Y.; Wang, X.; Fang, X. S.; Yao, J. N.; Bando, Y.; Golberg, D. One-Dimensional Inorganic Nanostructures: Synthesis, Field-Emission and Photodetection. *Chem. Soc. Rev.* **2011**, *40*, 2986−3004.
(17) Deng, K.; Li, L. CdS Nanoscale Photodetectors. *Adv. Mater.* **2014**, *26*, 2619−2635.
(18) Li, H. Q.; Wang, X.; Xu, J. Q.; Zhang, Q.; Bando, Y.; Golberg, D.; Ma, Y.; Zhai, T. Y. One-Dimensional CdS Nanostructures: A Promising Candidate for Optoelectronics. *Adv. Mater.* **2013**, *25*, 3017−3037.
(19) Gupta, S.; Mehta, B. R.; Satsangi, V. R. Size and Oxygen Passivation Induced Reversal of Photoconducting Behaviour in CdS Nanorods. *Nanotechnology* **2012**, *23*, 355702.
(20) Wei, T. Y.; Huang, C. T.; Hansen, B. J.; Lin, Y. F.; Chen, L. J.; Lu, S.-Y.; Wang, Z. L. Large Enhancement in Photon Detection Sensitivity via Schottky-Gated CdS Nanowire Nanosensors. *Appl. Phys. Lett.* **2010**, *96*, 013508.
(21) Li, L.; Wu, P.; Fang, X.; Zhai, T.; Dai, L.; Liao, M.; Koide, Y.; Wang, H.; Bando, Y.; Golberg, D. Single-Crystalline CdS Nanobelts for Excellent Field-Emitters and Ultrahigh Quantum-Efficiency Photodetectors. *Adv. Mater.* **2010**, *22*, 3161−3165.
(22) Kargar, A.; Sun, K.; Jing, Y.; Choi, C.; Jeong, H.; Jung, G. Y.; Jin, S.; Wang, D. L. 3D Branched Nanowire Photoelectrochemical Electrodes for Efficient Solar Water Splitting. *ACS Nano* **2013**, *7*, 9407−9415.
(23) Zhang, F.; Niu, S. M.; Guo, W. X.; Zhu, G.; Liu, Y.; Zhang, X. L.; Wang, Z. L. Piezo-Phototronic Effect Enhanced Visible/UV Photodetector of a Carbon-Fiber/ZnO-CdS Double-Shell Microwire. *ACS Nano* **2013**, *7*, 4537−4544.
(24) Heo, K.; Lee, H.; Park, Y.; Park, J.; Lim, H. J.; Yoon, D.; Lee, C.; Kim, M.; Cheong, H.; Park, J.; Jian, J.; Hong, S. Aligned Networks of Cadmium Sulfide Nanowires for Highly Flexible Photodetectors with Improved Photoconductive Responses. *J. Mater. Chem.* **2012**, *22*, 2173−2179.
(25) Xu, F.; Yuan, Y. F.; Han, H. J.; Wu, D. P.; Gao, Z. Y.; Jiang, K. Synthesis of ZnO/CdS Hierarchical Heterostructure with Enhanced Photocatalytic Efficiency under Nature Sunlight. *CrystEngComm* **2012**, *14*, 3615−3622.
(26) Zhang, C.; Tian, W.; Xu, Z.; Wang, X.; Liu, J. W.; Li, S. L.; Tang, D. M.; Liu, D. Q.; Liao, M. Y.; Bando, Y.; Golberg, D. Photosensing Performance of Branched CdS/ZnO Hetero-structures as Revealed by in Situ TEM and Photodetector Tests. *Nanoscale* **2014**, *6*, 8084−8090.
(27) Yang, X. F.; Zhuang, J. L.; Li, X. Y.; Chen, D. H.; Ouyang, G. F.; Mao, Z. Q.; Han, Y. X.; He, Z. H.; Liang, C. L.; Wu, M. M.; Yu, J. C. Hierarchically Nanostructured Rutile Arrays: Acid Vapor Oxidation Growth and Tunable Morphologies. *ACS Nano* **2009**, *3*, 1212−1218.
(28) Cheng, C. W.; Fan, H. J. Branched Nanowires: Synthesis and Energy Applications. *Nano Today* **2012**, *7*, 327−343.
(29) Zhou, W. C.; Peng, Y. H.; Yin, Y. L.; Zhou, Y.; Zhang, Y.; Tang, D. S. Broad Spectral Response Photodetector Based on Individual Tin-Doped CdS Nanowire. *AIP Adv.* **2014**, *4*, 123005.
(30) Li, G. H.; Jiang, Y.; Zhang, Y. G.; Lan, X. Z.; Zhai, T. Y.; Yi, G. C. High-Performance Photodetectors and Enhanced Field-Emission of CdS Nanowire Arrays on CdSe Single-Crystalline Sheets. *J. Mater. Chem. C* **2014**, *2*, 8252−8258.
(31) Gao, T.; Li, Q. H.; Wang, T. H. CdS Nanobelts as Photoconductors. *Appl. Phys. Lett.* **2005**, *86*, 173105.
(32) Lou, Z.; Li, L. D.; Shen, G. Z. High Performance Rigid and Flexible Ultraviolet Photodetectors with Single-Crystalline $ZnGa_2O_4$ Nanowires. *Nano Res.* **2015**, *8*, 2162−2169.
(33) Xie, X. M.; Shen, G. Z. Single-Crystalline In_2S_3 Nanowire-Based Flexible Visible-Light Photodetectors with an Ultra-High Photoresponse. *Nanoscale* **2015**, *7*, 5046−5052.
(34) Gong, X.; Tong, M. H.; Xia, Y. J.; Cai, W. Z.; Moon, J. S.; Cao, Y.; Yu, G.; Shieh, C. L.; Nilsson, B.; Heeger, A. J. High-Detectivity Polymer Photodetectors with Spectral Response from 300 to 1450 nm. *Science* **2009**, *325*, 1665−1667.
(35) Wu, P. C.; Dai, Y.; Ye, Y.; Yin, Y.; Dai, L. Fast-Speed and High-Gain Photodetectors of Individual Single Crystalline Zn_3P_2 Nanowires. *J. Mater. Chem.* **2011**, *21*, 2563−2567.
(36) Hu, X.; Zhang, X. D.; Liang, L.; Bao, J.; Li, S.; Yang, W. L.; Xie, Y. High-Performance Flexible Broadband Photodetector Based on Organolead Halide Perovskite. *Adv. Funct. Mater.* **2014**, *24*, 7373−7380.
(37) Wang, J. X.; Yan, C. Y.; Lin, M. F.; Tsukagoshib, K.; Lee, P. S. Solution-Assembled Nanowires for High Performance Flexible and Transparent Solar-Blind Photodetectors. *J. Mater. Chem. C* **2015**, *3*, 596−600.

DOI: 10.1021/acsami.5b06070
ACS Appl. Mater. Interfaces 2015, 7, 23507−23514